Desalination and Water Treatment
www.deswater.com

doi: 10.5004/dwt.2021.26743

214 (2021) 420–432
February

Kinetic, isotherm, and thermodynamic studies of Reactive Orange 13 adsorption onto activated carbon obtained from orange pulp

Sinem Güneş[a,*], Dilek Angın[b]

[a]*Department of Food Engineering, Institute of National Science, University of Sakarya, Esentepe Campus 54187, Sakarya, Turkey, email: sinemgunes.61@gmail.com*
[b]*Department of Food Engineering, Faculty of Engineering, University of Sakarya, Esentepe Campus 54187, Sakarya, Turkey, email: angin@sakarya.edu.tr*

Received 19 April 2020; Accepted 1 November 2020

ABSTRACT

Orange (*Citrus sinensis* L.) pulp, solid waste resulting from the production of citrus juice, was developed into activated carbon using zinc chloride at a 3:1 impregnation ratio with an activation temperature of 500°C. To determine the adsorption capacity, the prepared activated carbon was then utilized for the removal of dyestuff (Reactive Orange 13) from aqueous solutions. The resulting activated carbon had a high specific surface area of 1,779.48 m^2 g^{-1}. The experimental isotherm data were evaluated using the Langmuir, Freundlich, Temkin, and Dubinin–Radushkevich models. The experimental kinetic data were analyzed using the pseudo-first-order, pseudo-second-order, intra-particle diffusion, and Elovich models. The results obtained from the isotherm and kinetic studies were well explained, respectively, by the Langmuir and pseudo-second-order models. Thermodynamic parameters were computed, and the results obtained revealed that the present adsorption is a spontaneous and endothermic adsorption process. These findings indicate that orange pulp activated carbon can be effectively utilized as an inexpensive adsorbent to remove dyestuff from an aqueous solution.

Keywords: Activated carbon; Adsorption; Dyestuff; Food industry waste; Orange pulp

1. Introduction

As a result of the development of industry and the rapid growth of the world population, the demand for fresh water is continuously increasing [1]. Thus, the treatment of wastewater, which is industrial and municipal, has become one of the main topics of countries. Most of the pollution in wastewater is composed of various chemical compounds. Pesticides, heavy metals, dyes, etc. are among important contaminants. Exposure to these chemicals causes damage to both human health and the environment [2].

Dyes are used to coloring a wide variety of products, such as in the textile, cosmetic, food, plastic, paint, and paper industries. Some of the synthetic dyes used in the coloring process end up in industrial wastewater [3], which can cause environmental pollution and pose a danger to human health. Wastewater polluted with containing dyes has low light permeability, which adversely affects aquatic life [4]. Some dyes are also toxic and many remain in wastewater for an extended period owing to their low biodegradability and photodegradability, and stability to oxidation agents [5]. Thus, synthetic dyes must be removed from wastewater before it is discharged into waterways.

Technologies used to remove dye from effluents can be classified into three categories: physical, chemical, and biological. Various methods are applied, such as oxidation, chemical precipitation, adsorption, membrane filtration, ion exchange, and aerobic and anaerobic microbial degradation [4]. Each of these methods has limitations, such as high cost,

* Corresponding author.

disposal problems [3,4]. Furthermore, owing to the complex nature of wastewater, none of these methods can achieve effective dye removal on their own [3]. Adsorption has the best potential in terms of its low cost, easy operation, and simple design. Activated carbon is among the most commonly used adsorbents [6] and has found extensive applications in areas such as purification, chemical recovery, and the removal of colors, metals, odors, or tastes from wastewater owing to the high surface area, well-developed internal pore structure and various surface functional groups [7].

Two different processes are employed for the production of activated carbon: physical activation and chemical activation. Under the physical treatment, the precursor is carbonized at high temperatures (700°C–1,000°C) employing oxidizing agents, such as CO_2, air, or water. For chemical activation, the precursor is firstly impregnated with chemical agents ($ZnCl_2$, H_3PO_4, H_2SO_4, KOH, K_2CO_3, etc.), which improves the pore structure of the material, then the impregnated material is carbonized at a low temperature under an inert atmosphere [8,9]. However, the high price of commercially available activated carbon limits its use. Therefore, many researchers have begun to look for cheaper ways of producing activated carbon and have reported that agricultural waste, such as sour cherry stones [10], olive-waste cake [11], wood apple shells [12], sesame stalks [13], tomato processing solid waste [14], and sugarcane bagasse [15], could be used for activated carbon production.

In various industries (food, textile, etc.), waste is generated during the processing of raw materials. Elimination or disposal of this waste causes serious environmental problems and financial costs to the industry. The disposal and treatment of waste are significant problems in the food industry. During the processing of agricultural raw materials in the food industry, a large amount of liquid (wastewater, whey) and solid (shell, peel, and pulp) waste material is formed [16]. These residues have substantial impacts on the environment. Thus, the management of waste materials is of great importance.

Turkey ranks ninth globally in orange production with 1.9 million tons in 2018 [17]. According to the USDA report published in July 2019, approximately 0.5% of fresh oranges are processed into fruit juice in Turkey [18]. After the production of orange juice, a large amount of waste (peel, pulp, seeds, etc.), amounting to nearly half of the fresh orange weight, is obtained [19]. Thus, in the current study activated carbon was derived from the orange pulp, obtained as solid waste during fruit juice processing, by chemical activation with zinc chloride ($ZnCl_2$). The adsorption capacity of the produced activated carbon was investigated by the removal of Reactive Orange 13 (RO-13) from aqueous solutions. The effect of the adsorbent dosage, initial pH, and initial concentration of the dyestuff solution on the adsorption was examined in a batch system. Isotherm, kinetic, and thermodynamic studies were performed.

2. Materials and methods

2.1. Materials

Orange (*Citrus sinensis* L.) pulp, which is waste from the fruit juice industry waste consisting of a mixture of peel, segment walls, and seeds, was procured from Limkon Food Industry and Trade Inc., Adana, Turkey. The orange pulp was first dried at room temperature and then in an oven at 105°C ± 3°C. The dried pulp was then crushed to a size of 1–2 mm. The pulp powder was kept at room conditions in a glass jar for further use.

RO-13 dye with a Color Index number (C.I. number) of 18,270 was procured from SARAR Textile Factory (Eskişehir, Turkey). RO-13 has a molecular formula of $C_{24}H_{15}ClN_7Na_3O_{10}S_3$ and a molecular weight of 762.04 g mol^{-1}. The dyestuff stock solution was obtained by dissolving 1 g of RO-13 in 1 L of deionized water. The solution was then shaken well and kept in a volumetric flask for further study.

Zinc chloride ($ZnCl_2$), used as a chemical agent, and hydrochloric acid (HCl) and sodium hydroxide (NaOH), used for adjusting the pH of the dye solutions, were purchased from Merck (Darmstadt, Germany). All chemicals employed in this study were of analytical grade.

2.2. Preparation of activated carbon

The optimum activated carbon production conditions giving the highest BET surface area were determined in a previous study as follows: 500°C activation temperature and 3:1 impregnation ratio ($ZnCl_2$:orange pulp). Therefore, activated carbon obtained under these conditions was used in subsequent adsorption experiments [20].

For chemical activation, 60 g of $ZnCl_2$ was dissolved in about 250 mL of deionized water in a beaker, and then 20 g of orange pulp was added to the $ZnCl_2$ solution. To maintain a full reaction between the $ZnCl_2$ and the orange pulp, the mixture was kept on a magnetic stirrer (WiseStir MSH-20A, Daihan Scientific Co., Korea) at 80°C–85°C for 24 h. The obtained reaction mixture was filtered, and the collected solids were dried at 150°C ± 3°C for 24 h and then ground in a blender (Waring). The ground samples were weighed into a ceramic crucible and placed in a tubular reactor (Protherm PTF-12) for carbonization. The samples were heated from room temperature to the final treatment temperature (500°C) under nitrogen gas flow (200–300 cm^3 min^{-1}) with a heating rate of 5°C min^{-1} and then held for 2 h at 500°C. After carbonization, the samples were cooled down to room temperature under flowing nitrogen. The cooled samples were boiled at approximately 90°C in 0.1 L of 1 N HCl solution for 1 h, then rinsed with hot and cool deionized water to remove organic and mineral matters until the pH of the remaining water reached 6–7, and then dried at 105°C for 24 h.

2.3. Characterization of orange pulp and activated carbon

The moisture, volatile, and ash content of the orange pulp and activated carbon were determined using American Society for Testing and Materials (ASTM) standard test methods. The fixed carbon content was calculated by difference. The proximate analyses of orange pulp and activated carbon were carried out using a LECO CHNS 932 elemental analyzer with ±0.4% accuracy (LECO Instruments, Michigan, USA). The oxygen content was calculated by difference. The characteristics of the orange pulp and activated carbon are summarized in Table 1 [21].

The N_2 adsorption/desorption isotherms at 77 K were measured using an automated adsorption instrument

Table 1
Characteristics of the orange pulp raw material and activated carbon [21]

Properties	Methods	Orange pulp	Methods	Activated carbon
Proximate analysis (wt.%)				
Moisture content (wt.%)	ASTM D 2016-74	3.70	ASTM D 2867-09	8.37
Volatile matter	ASTM D 5832-98	82.70	ASTM E 897-82	9.18
Ash	ASTM D 1102-84	2.80	ASTM D 2866-11	0.57
Fixed carbon	By difference	14.50	By difference	90.25
Ultimate analysis (wt.%)				
Carbon	LECO instruments	45.05	LECO instruments	56.57
Hydrogen		6.29		2.68
Nitrogen		1.66		2.77
Sulfur		0.03		0.08
Oxygen	By difference	46.97	By difference	37.90
Surface properties				
BET surface area ($m^2\ g^{-1}$)		0.704		1,779.48
Micropore area ($m^2\ g^{-1}$)		–		1,383.20
Total pore volume ($cm^{-3}\ g^{-1}$)		–		1.343
Micropore volume ($cm^{-3}\ g^{-1}$)		–		1.100
Average pore diameter (nm)		–		1.98

(Nova 4000E, Quantachrome Instruments) to assess the surface area and pore structure of the activated carbon. The N_2 adsorption data for the activated carbon were analyzed using Quantachrome NovaWin2 software to assess the surface area, pore volume, and pore size distribution. Adsorption data were measured in the relative pressure (P/P_0) range from 10^{-5} to 1. The activated carbon sample was degassed in a vacuum at 300°C for 5 h. The apparent surface area was determined by applying the Brunauer–Emmett–Teller (BET) equation within the relative pressure range of 0.01–0.2. The micropore volume was calculated using the Dubinin–Radushkevich (D–R) method. The quantity of N_2 adsorbed at relative pressures close to unity (≈0.99) corresponds to the total adsorbed quantity in both the micropores and the mesopores; subsequently, the volume of the mesopores is provided by subtracting the micropore volume from the total quantity [22].

2.4. Adsorption studies

Experimental parameters were determined considering the adsorption studies reported in the literature [12,23,24]. The adsorption studies were conducted using a batch-type process. The effects of initial adsorbent dosage, initial pH value, initial dyestuff concentration, contact time, and temperature on the adsorption were studied. The dyestuff solutions were prepared from the stock solution. The batch process was performed by placing 0.1 L of dyestuff solution in a 250 mL capped volumetric flask with a fixed adsorbent dosage and shaking at 120 rpm for 24 h in a water bath (GFL-1083). The initial pH of the dyestuff solution was adjusted by using solutions of HCl and NaOH and a pH meter (Mettler–Toledo S220, Columbus OH, USA). The samples were filtered after the adsorption process and the concentration of dyestuff remaining was determined using a spectrophotometer (Shimadzu UV-Vis 1240) at 217 nm. The relationship between the concentration (C) and absorbance (x) was $C = x/0.0301$. The removal percentage (%) and the amount of dyestuff in the adsorbent at equilibrium (q_e, mg g^{-1}) were determined using Eqs. (1) and (2), respectively:

$$\text{Removal}\,(\%) = \frac{(C_0 - C_e)}{C_0} \times 10 \tag{1}$$

$$q_e = \frac{(C_0 - C_e)}{m} \times V \tag{2}$$

where C_0 and C_e (mg L^{-1}) are the initial and equilibrium dyestuff concentration, (mg L^{-1}), respectively, m is the mass of activated carbon (g), and V is the volume of solution (L) [13,25,26].

2.5. Adsorption isotherms

Adsorption isotherms are used to predict how much solute can be adsorbed by activated carbon at a constant temperature at equilibrium and demonstrate the equilibrium relationship between the adsorbent and the adsorbate [27,28]. The adsorption experiments were carried out at 298, 308, and 318 K using the optimum activated carbon dosage with 0.1 L RO-13 solutions of various initial concentrations (50, 100, 150, 200, 250, and 300 mg L^{-1}) at the optimum pH of 2. After adsorption, the activated carbon samples were filtered, and a UV-vis spectrophotometer was utilized to determine the dyestuff concentrations. The experimental equilibrium data were fitted using four isotherm models, namely Langmuir [29], Freundlich [30],

Dubinin–Radushkevich (D–R) [31], and Temkin [32]. The equations for these adsorption isotherms are listed in Table 2.

2.6. Adsorption kinetics

The adsorption mechanism and the time to reach equilibrium can be determined by kinetic studies [33]. Kinetic studies were conducted using 0.1 L of RO-13 solution with an initial dye concentration of 100 mg L^{-1} at optimum pH and agitating with the optimum activated carbon dosage at 120 rpm at 298, 308, and 318 K. At the end of the predetermined shaking time, each sample was filtered, and the dyestuff concentrations were determined using a UV-vis spectrophotometer. The obtained experimental data were fitted using four models: pseudo-first-order [34], pseudo-second-order [35], intra-particle diffusion [36], and Elovich [37]. The equations for these models are summarized in Table 2.

2.7. Thermodynamic studies

The thermodynamic parameters of Gibbs free energy change ($\Delta G°$), enthalpy change ($\Delta H°$), and entropy change ($\Delta S°$) were calculated to assess the nature and feasibility of the adsorption. Eq. (3) was used to calculate the $\Delta G°$:

$$\Delta G° = -RT\ln K \tag{3}$$

where R (8.314 J $mol^{-1}K^{-1}$) is the gas constant, T (K) is the temperature, and K is the thermodynamic equilibrium constant. The equilibrium constant (K) is calculated using Eq. (4):

$$K = \frac{q_e}{C_e} \tag{4}$$

The relation between $\Delta G°$, $\Delta S°$, and $\Delta H°$ can be described as:

$$\Delta G° = \Delta H° - T\Delta S° \tag{5}$$

Eq. (3) can be written as:

$$\ln K = -\frac{\Delta G°}{RT} = -\frac{\Delta H°}{RT} + \frac{\Delta S°}{R} \tag{6}$$

The values $\Delta H°$ (kJ mol^{-1}) and $\Delta S°$ (kJ mol^{-1} K^{-1}) are obtained from the slope and intercept of ln$K$ vs. $1/T$, respectively [38,39].

The thermodynamic studies were conducted at different adsorption temperatures by employing the optimum activated carbon dosage and 0.1 L of 100 mg L^{-1} RO-13 solution and agitating at 120 rpm for 24 h. After adsorption, the samples were filtered, and a UV-vis spectrophotometer was utilized to quantify the dyestuff concentrations. The thermodynamic parameters were calculated using Eq. (6).

2.8. Error determination

The isotherm and kinetic models were evaluated according to the coefficient of determination (R^2) and the root mean square error (RMSE). RMSE is calculated using Eq. (7) [40]:

$$\text{RMSE} = \sqrt{\frac{1}{n}\Sigma\left(q_{\text{cal}} - q_{\text{exp}}\right)^2} \tag{7}$$

where q_{cal} (mg g^{-1}) and q_{exp} (mg g^{-1}) are the calculated and experimental RO-13 adsorption capacities, respectively, and n is the number of samples. Higher R^2 and lower RMSE values indicate better fitting of the models.

3. Results and discussion

3.1. Characterization of the activated carbon

Table 1 presents the proximate and ultimate analysis results and the surface properties of the orange pulp and the activated carbon. According to the results of the analysis, the volatile matter content in the activated carbon decreased compared to orange pulp as a result of its release during the heat treatment step in the activation process [26]. The carbon content increased with a consequent decrease in the hydrogen and oxygen contents after the activation process. It was observed that the fixed carbon content of the activated carbon increased from 14.50% to 90.25%. The high fixed carbon content shows that the obtained activated carbon has good potential as an adsorbent while the high volatile matter and low ash contents of the orange pulp indicate that it is suitable for use can be utilized as a raw material for the production of activated carbon [41]. A high surface area or micropore volume is an important feature in adsorbent selection and is important for obtaining a high adsorption capacity. The presence of micropores contributes to the increase of the adsorption capacity, increasing the number of adsorption sites [42,43]. The pore structure characteristics of the activated carbon are presented in Table 1. The surface area of the obtained activated carbon was 1,779 m^2 g^{-1} and the micropore volume was determined to be 1.343 cm^3 g^{-1}. Most of the activated carbon (≈78%) consists of micropores. When these surface properties are compared with those of activated carbons obtained from different raw materials, the obtained activated carbon shows good potential for application as an adsorbent [9,14,15,24,41,44,45].

3.2. Effect of initial pH

The pH of the dyestuff solution is a considerable parameter that affects both the adsorption capacity and surface charge of the activated carbon [5]. The effect of the initial pH of the dyestuff solution on RO-13 removal by activated carbon was examined using various pH values (1, 2, 4, 5, 6, 7, 8, 10, and 12) and the results are shown in Fig. 1. The removal of RO-13 ranged from 94.80% to 98.14% at low pH (2–6), while above pH 6.0 the percentage removal of RO-13 decreased to 83.06%. RO-13 acts as an anionic charged molecule in an aqueous solution since it has three sulfonate groups. In acidic solution, the dyestuff can also behave as a cationic charged molecule owing to the protonation of the amino group of RO-13 [44]. When the pH of the aqueous solution is low, the surface of the activated carbon is positively charged. Conversely, the surface of the

Table 2
Adsorption isotherms and kinetic models and equations

Model	Linearized form of equation	Plot	Parameter	References
Adsorption isotherms				
Langmuir	$\frac{C_e}{q_e}=\frac{C_e}{Q_0}+\frac{1}{Q_0K_L}$ $R_L=\frac{1}{\left(1+K_LC_0\right)}$	$\frac{C_e}{q_e}$ vs. C_e	q_e (mg g^{-1}): equilibrium dye concentration on the adsorbent; C_e (mg g^{-1}): equilibrium dye concentration in the solution; Q_0 (mg g^{-1}): monolayer adsorption capacity of the adsorbent; K_L (L mg^{-1}): Langmuir adsorption constant; R_L: dimensionless constant called separation factor, which indicates the adsorption nature;	[24,29]
Freundlich	$\log q_e=\log K_F+\left(\frac{1}{n}\right)\log C_e$	$\log q_e$ vs. $\log C_e$	K_F (mg g^{-1}) (L mg^{-1})$^{1/n}$: Freundlich adsorption constant; n: Freundlich constant, which gives an indication of how favourable an adsorption process is;	[30,39]
D–R	$\ln q_e=\ln q_m-B\varepsilon^2$ $\varepsilon=RT\ln\left(1+\frac{1}{C_e}\right)$ $E=\frac{1}{\sqrt{2B}}$	$\ln q_e$ vs. ε^2	q_m (mg g^{-1}): adsorption capacity; B (mol^2 J^{-2}): constant related to the sorption energy; ε: Polanyi potential, which is related to the equilibrium concentration; R (J mol^{-1} K^{-1}): gas constant (8.314); T (K): absolute temperature; E (kJ mol^{-1}): constant gives information about the type of adsorption mechanism;	[13,31]
Temkin	$q_e=B_1\ln A+B_1\ln C_e$ $B_1=\frac{RT}{b}$	q_e vs. $\ln C_e$	B_1 (J mol^{-1}): Temkin constant related to heat of adsorption; A (L mg^{-1}): equilibrium binding constant;	[32,40]
Adsorption kinetics				
Pseudo-first-order	$\log\left(q_e-q_t\right)=\log q_e-\frac{k_1t}{2.303}$	$\log(q_e-q_t)$ vs. t	q_t (mg g^{-1}): amount of adsorbate adsorbed at time t; k_1 (min^{-1}): pseudo-first-order rate constant; k_2 (g mg^{-1} min^{-1}): pseudo-second-order rate constant;	[34,41]
Pseudo-second-order	$\frac{t}{q_t}=\frac{1}{k_2q_e^2}+\frac{t}{q_e}$	$\frac{t}{q_t}$ vs. t	k_p (mg g^{-1} min$^{-1/2}$): intra-particle diffusion rate constant; C (mg g^{-1}): constant that gives an idea about the thickness of the boundary layer;	[35,38]
Intra-particle diffusion	$q_t=k_pt^{1/2}+C$	q_t vs. $t^{1/2}$	α (mg g^{-1} min^{-1}): initial adsorption rate; β (g mg^{-1}): parameter is related to extent of surface coverage and activation energy for chemisorption;	[36,42]
Elovich	$q_t=\frac{1}{\beta}\ln\left(\alpha\beta\right)+\frac{1}{\beta}\ln t$	q_t vs. $\ln t$		[37,43]

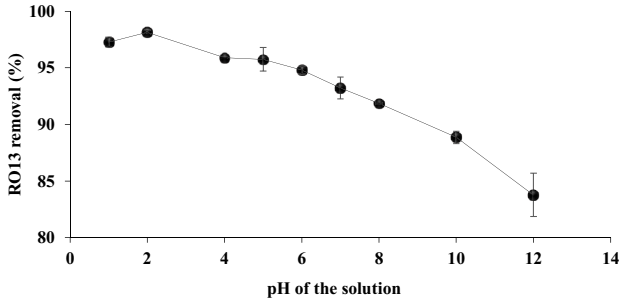

Fig. 1. Effect of solution pH on the adsorption of RO-13 (amount of activated carbon: 0.2 g, C_0: 100 mg L^{-1}, shaking rate: 120 rpm, and temperature: 298 K, 24 h).

activated carbon is negatively charged when the pH is high (basic conditions). The activated carbon surface is positively charged at low pH. Therefore, electrostatic attraction occurs between the positively charged surface of the carbon and the anionic dye molecule, thus resulting in maximum RO-13 uptake. Meanwhile, at high pH, electrostatic repulsion occurs between the negatively charged surface of the activated carbon and the negatively charged dye molecules [5,44]. The RO-13 adsorption of the activated carbon was found to be highly dependent on the pH of the solution. The maximum RO-13 adsorption was observed at pH 2.0, which was utilized for the subsequent experiments. Similar findings have been reported from other studies [5,24,28].

3.3. Effect of adsorbent dosage

The influence of the dose of activated carbon on the removal of RO-13 is exhibited in Fig. 2. The results clearly show that the removal of RO-13 increased from 74.55% to 96.28% as the dose increased from 0.05 to 0.2 g/0.1 L, then remained almost constant. However, the amount of dyestuff adsorbed per unit decreased from 149.10 to 12.07 mg g^{-1}. The increased removal efficiency was a consequence of increasing the number of accessible and available adsorption sites and surface area by increasing the adsorbent dosage. The subsequent decrease in the uptake of RO-13 per unit of activated carbon is mainly due to the increase in the unsaturated adsorption sites [45]. In addition, this decrease can be ascribed to the aggregation or overlapping of the adsorption sites with increasing activated carbon dosage [46]. An activated carbon dose of 0.2 g/0.1 L was utilized for the subsequent studies.

3.4. Effect of initial RO-13 concentration

The effect of the initial RO-13 concentration on the adsorption was investigated with concentrations ranging from 50 to 300 mg L^{-1} at 298 K. Fig. 3 shows that the adsorption capacity of the activated carbon made from orange pulp increased with an increase in the initial the RO-13 concentration. The percentage RO-13 removal decreased as the initial RO-13 concentration increased. This could be attributed to the limited number of available active sites on the surface of the activated carbon with the higher initial RO-13 concentration [47].

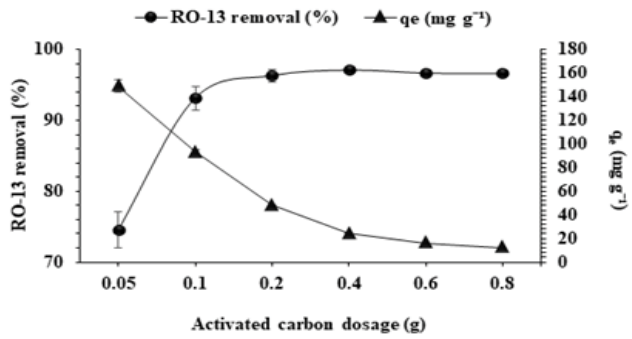

Fig. 2. Effect of adsorbent dosage on the adsorption of RO-13 onto activated carbon and the amount of RO-13 adsorbed per unit activated carbon (C_0: 100 mg L^{-1}, initial pH: 2.0, shaking rate: 120 rpm, and temperature: 298 K, 24 h).

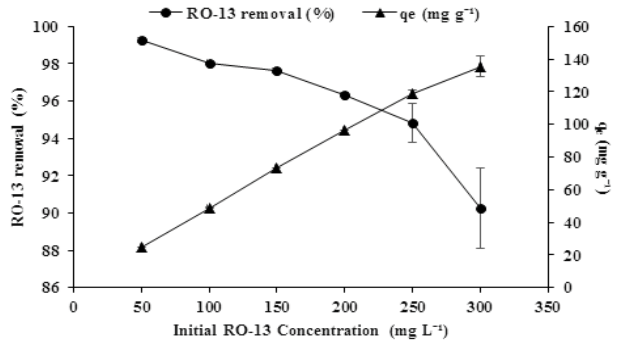

Fig. 3. Effect of initial RO-13 concentration on the adsorption of RO-13 (amount of activated carbon: 0.2 g, initial pH: 2.0, shaking rate: 120 rpm, and temperature: 298 K, 24 h).

3.5. Effect of temperature and contact time

The adsorption of RO-13 with varying contact times (15, 30, 45, 60, 90, 120, 180, 240, 300, 360, 420, 480, and 540 min) is shown in Fig. 4. The removal percentage of RO-13 adsorption increased with increasing contact time for all three temperatures. Approximately 38%, 44%, and 51% dyestuff removal was achieved in the first 15 min at 298, 308, and 318 K, respectively. The adsorption of RO-13 was rapid within the first 60 min, then it progressed gradually until reaching equilibrium. Adsorption equilibrium was achieved within 360 min at all temperatures. The positively charged surface of the adsorbent led to fast electrostatic adsorption of anionic RO-13 from the solution. This allowed adsorption to occur rapidly in the initial contact period [28]. In addition, the percentage of dye removal was increased with increasing initial contact time due to the availability of the initially accessible surface area [47]. The removal of RO-13 increased from 94% to 98% as the adsorption temperature was increased from 298 to 318 K for an RO-13 concentration of 100 mg L^{-1}. The adsorption capacity of the activated carbon increased with increasing temperature, indicating that the adsorption process is endothermic. This increase may be owing to the increased mobility of the dye molecules and an increase in the number of active adsorption sites at higher temperatures [4].

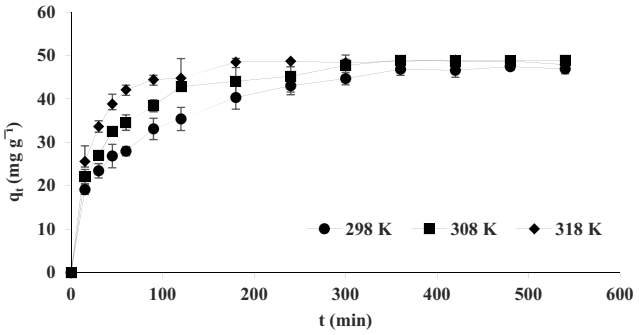

Fig. 4. Effect of temperature on the adsorption of RO-13 (amount of activated carbon: 0.2 g, C_0: 100 mg L^{-1}, initial pH: 2.0, and shaking rate: 120 rpm).

3.6. Adsorption isotherms

The adsorption equilibrium data for RO-13 were compared with the data obtained using the Langmuir, Freundlich, D–R, and Temkin isotherm models, as shown in Fig. 5. In addition, the RO-13 adsorption isotherm curves obtained for the activated carbon are presented in Figs. S1 and S2. The parameters for the isotherm models at the different temperatures and the values of R^2 and RMSE calculated from the experimental data are listed in Table 3.

Based on the highest R^2 and lowest RSME values, the Langmuir model fitted the experimental data for the adsorption of RO-13 better than the other models. The Langmuir isotherm model proposes that the adsorption of RO-13 on orange pulp activated carbon proceeds as a homogeneous monolayer [48]. The value of R_L indicates the adsorption nature to be either unfavorable (R_L > 1), linear (R_L = 1), favorable (0 < R_L < 1), or irreversible (R_L = 0) [39]. The calculated R_L values were found to be between 0.008 and 0.06 at different temperatures. According to these values, the adsorption of RO-13 is a favorable process. Furthermore, the Langmuir isotherm parameters, Q_0 and K_L, increased with increasing temperature. The maximum adsorption capacity increased from 147.06 to 263.16 mg g^{-1} when the temperature was increased from 298 to 318 K. These results show that the adsorption process must be endothermic.

The Freundlich constants n and K_F give an indication of the favorability of the adsorption process and the adsorption capacity of the adsorbent, respectively. If 1/n < 1, it indicates favorable adsorption [5]. At all three temperatures used in this study, 1/n was smaller than 1. Moreover, K_F increased with temperature. Thus, higher temperatures are favorable for RO-13 removal.

To differentiate between physical and chemical adsorption of RO-13, the D–R isotherm model was employed [49]. The D–R model showed the worst fit to the experimental data. The constant E provides information regarding the adsorption type. If the E value is within 8–16 kJ mol^{-1}, the adsorption mechanism is characterized as chemical adsorption [50], whereas for values of E < 8 kJ mol^{-1}, the adsorption mechanism is physical adsorption [49]. The calculated values of E indicate that RO-13 was physically adsorbed onto the activated carbon.

The Temkin isotherm model considers the effect of indirect adsorbate–adsorbate interactions on the adsorption process [51]. The experimental data was found to be suitable for the Temkin isotherm model. The Temkin isotherm constant indicates that the heat of adsorption (B_1) increased with temperature, suggesting endothermic adsorption.

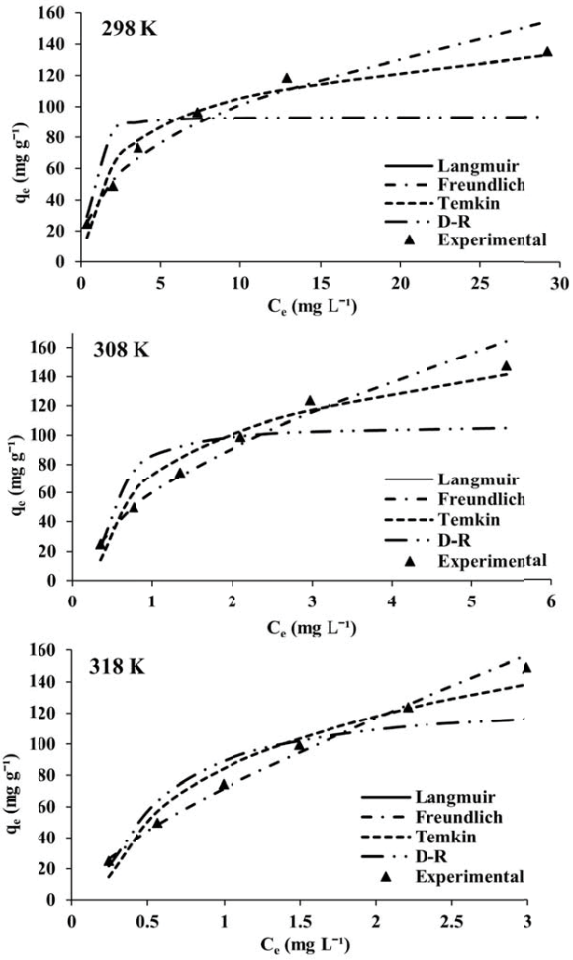

Fig. 5. Adsorption isotherms for RO-13 at different temperatures (amount of activated carbon: 0.2 g, C_0: 50–300 mg L^{-1}, initial pH: 2.0, and shaking rate: 120 rpm, 24 h).

The maximum adsorption capacity of the orange pulp activated carbon was compared with some other adsorbents reported in the literature, as shown in Table 4. The adsorption capacity of the orange pulp activated carbon was found to be higher than that of other reported adsorbents. Thus, the activated carbon prepared in this work is an efficient adsorbent with good capacity for the removal of dyestuff from aqueous solutions and can be used as an affordable adsorbent for the treatment of wastewater.

3.7. Adsorption kinetics

The calculated parameters and the R^2 and RMSE values for the pseudo-first-order, pseudo-second-order, intraparticle diffusion, and Elovich models at different temperatures are listed in Table 5 and the results are shown in Fig. 6. In addition, the RO-13 adsorption kinetic curves obtained for the activated carbon are included in Figs. S3

Table 3
Isotherm models and parameters for the removal of RO-13

Isotherm models	Temperature (K)	Parameters				
Langmuir		Q_0 (mg g^{-1})	K_L (L mg^{-1})	R_L	R^2	RSME
	298	147.06	0.308	0.011–0.0611	0.9945	8.16
	308	222.22	0.375	0.051–0.0088	0.9938	9.32
	318	263.16	0.413	0.008–0.046	0.9921	8.81
Freundlich			$1/n$	K_F (mg g^{-1}) (L mg^{-1})$^{1/n}$	R^2	RSME
	298		0.409	39.62	0.9788	15.46
	308		0.5997	60.03	0.8251	13.16
	318		0.7081	72.41	0.9951	10.94
D–R		q_s (mg g^{-1})	B (mol^2 kJ^{-2})	E (kJ mol^{-1})	R^2	RSME
	298	93.20	0.1	2.236	0.7451	26.28
	308	106.44	0.08	2.659	0.8251	26.15
	318	122.51	0.1	2.236	0.9159	17.19
Temkin			A (L g^{-1})	B_1	R^2	RSME
	298		5.121	26.84	0.9622	10.53
	308		5.762	41.13	0.9603	18.05
	318		5.703	48.83	0.9655	11.02

Table 4
Comparison of the maximum adsorption capacity of the orange pulp activated carbon with other adsorbents

Adsorbent	Dye	Temperature (K)	q_{max} (mg g^{-1})	Reference
Wood apple shell activated carbon	Congo Red	298	83.3	[12]
Phragmites australis activated carbon	Methyl Orange	303	217.4	[54]
Rice hull activated carbon	Eriochrome Black T	298	160.4	[52]
Alginate–montmorillonite–polyaniline nanocomposite	Reactive Orange 13	–	111.1	[55]
$NiFe_2O_4$ nanoparticles	Reactive Orange 13	298	243.9	[56]
Orange pulp activated carbon	Reactive Orange 13	318	263.2	Present study

and S4. It can be seen in Table 5 that the pseudo-second-order model shows a good fit with experimental data. The pseudo-second-order model gave the highest R^2 values, ranging from 0.998 to 0.999, and the RSME values are lower than those observed for the pseudo-first-order model. Moreover, the q_e values (q_e^{cal}) calculated using the pseudo-second-order model are consistent with experimental data (q_e^{exp}). Similar observations were also reported by other researchers [48,52,40].

The Elovich model assumes that the active sites of adsorbents are heterogeneous and the adsorption occurs mainly by chemisorption [9,46]. The constant α is related to the rate of chemisorption and β is related to the surface coverage. The values of α and β both increased with temperature, indicating that RO-13 uptake onto activated carbon occurs predominantly by chemisorption.

The intra-particle diffusion model was applied to describe the diffusion mechanism. If the adsorption process is only regulated by intra-particle diffusion, the graph of q_t vs. $t^{1/2}$ is linear passing through the origin. However, if this plot does not pass through the origin, the rate of adsorption may be governed by mechanisms other than or in addition to intra-particle diffusion [53]. As shown in Fig. 6, the curves did not pass through the origin for each temperature, which implies that intra-particle diffusion is not the only rate-determining step for the adsorption of RO-13; external mass transfer might also be important in the adsorption process.

3.8. Thermodynamic studies

Thermodynamic parameters were calculated for all initial concentrations of RO-13 and a similar situation was observed for all concentrations (Table 6). The negative values of $\Delta G°$ demonstrate that the adsorption process is spontaneous and thermodynamically favorable [57,58] while the positive values of $\Delta H°$ show that the process of RO-13 adsorption is endothermic [58]. As can be seen in Table 6, the $\Delta S°$ values were positive for the adsorption of RO-13, which indicates increasing disorder and randomness at the solid-solution interface [59,60].

4. Conclusion

The feasibility of orange pulp activated carbon for removing RO-13 from aqueous solution was investigated

in the current study. The influence of the pH, concentration, temperature, contact time, and adsorbent dose was studied in batch experiments. The results showed that the adsorption of RO-13 was highest at pH 2. The adsorption capacity was found to increase with increasing initial solution concentration, temperature, and contact time while it decreased with increasing adsorbent dosage. Equilibrium data were best fitted by the Langmuir isotherm with a maximum monolayer adsorption capacity of 263.16 mg g^{-1}, which is comparable with many of the adsorbents mentioned in the literature. The adsorption kinetics of RO-13 onto orange pulp activated carbon obeyed the pseudo-second-order model and the intra-particle diffusion model suggested that intra-particle diffusion was not the only rate-controlling step. Thermodynamic investigations also revealed that the dyestuff adsorption was endothermic and spontaneous. From the results of the present study, it was concluded that the orange pulp activated carbon provides a novel and cost-effective treatment for wastewater.

Table 5
Kinetic parameters for the removal of RO-13

Solution temperature (K)	298	308	318
q_e^{exp} (mg g^{-1})	49.012	49.618	49.718
Pseudo-first-order			
k_1 (min^{-1})	0.006	0.009	0.0055
q_e^{cal} (mg g^{-1})	27.638	23.659	9.770
R^2	0.955	0.919	0.682
RSME	20.67	24.71	38.47
Pseudo-second-order			
k_2 (g mg^{-1} min^{-1})	0.0238	0.0371	0.089
q_e^{cal} (mg g^{-1})	51.020	51.546	49.75
R^2	0.998	0.999	0.999
RSME	16.16	13.32	8.89
Intra-particle diffusion			
k_p (mg $g^{-1}min^{-1/2}$)	1.47	1.2769	0.8936
C (mg g^{-1})	17.225	23.557	31.747
R^2	0.935	0.861	0.669
RSME	2.45	3.26	3.97
Elovich			
α (mg g^{-1} min^{-1})	4.5402	10.7572	82.0526
β (g mg^{-1})	0.1156	0.1289	0.1732
R^2	0.988	0.971	0.855
RSME	1.09	1.53	2.63

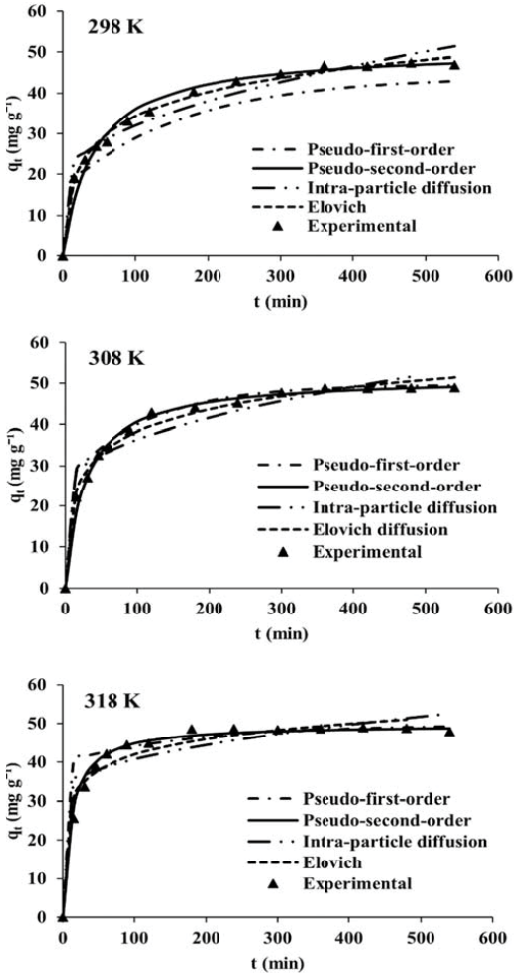

Fig. 6. Adsorption kinetic models for RO-13 at different temperatures (amount of activated carbon: 0.2 g, C_0: 100 mg L^{-1}, initial pH: 2.0, and shaking rate: 120 rpm).

Table 6
Thermodynamic parameters for the adsorption of RO-13

Initial dyestuff concentration (mg L^{-1})	ΔG° (kJ mol^{-1})			ΔH° (kJ mol^{-1})	ΔS° (kJ mol^{-1} K^{-1})
	Temperature (K)				
	298	308	318		
50	–10.45	–10.92	–12.26	16.38	0.089
100	–7.95	–10.69	–11.84	50.18	0.196
150	–7.48	–10.27	–11.41	51.22	0.198
200	–6.40	–9.85	–11.09	63.87	0.237
250	–5.49	–9.54	–10.65	71.76	0.261
300	–3.79	–8.45	–10.32	93.93	0.329

Acknowledgments

The authors gratefully acknowledge Adana Limkon Food Industry and Trade, Inc. (Turkey) for supplying the orange pulp. Also, we would like to thank the editing team of Kalite Editing Services for proofreading of the current manuscript.

Symbols

q_e	—	Equilibrium dye concentration on the adsorbent, mg g^{-1}
C_e	—	Equilibrium dye concentration in the solution, mg g^{-1}
V	—	Volume of solution, L
m	—	Mass of the activated carbon, g
Q_0	—	Monolayer adsorption capacity of the adsorbent, mg g^{-1}
K_L	—	Langmuir adsorption constant, L mg^{-1}
R_L	—	Dimensionless constant that called separation factor indicates the adsorption nature
K_F	—	Freundlich adsorption constant, (mg g^{-1}) (L $mg^{-1})^{1/n}$
n	—	Freundlich constant that give an indication of how favorable the adsorption process
q_m	—	Adsorption capacity, mg g^{-1}
B	—	Constant related to the sorption energy, mol^2 J^{-2}
ε	—	Polanyi potential which is related to the equilibrium concentration
R	—	Gas constant, 8.314 J $mol^{-1}K^{-1}$
T	—	Absolute temperature, K
E	—	Constant gives information about the type of adsorption mechanism, kJ mol^{-1}
B_1	—	Temkin constant related to heat of adsorption, J mol^{-1}
A	—	Equilibrium binding constant, L mg^{-1}
q_t	—	Amount of adsorbate adsorbed at time t, mg g^{-1}
k_1	—	Pseudo-first-order rate constant, min^{-1}
k_2	—	Pseudo-second-order rate constant, g $mg^{-1}min^{-1}$
k_p	—	Intraparticle diffusion rate constant, mg $g^{-1}min^{-1/2}$
C	—	Constant that gives an idea about the thickness of the boundary layer, mg g^{-1}
α	—	Initial adsorption rate, mg $g^{-1}min^{-1}$
β	—	Parameter is related to extent of surface coverage and activation energy for chemisorption, g mg^{-1}
$\Delta G°$	—	Gibbs free energy change, kJ mol^{-1}
$\Delta H°$	—	Enthalpy change, kJ mol^{-1}
$\Delta S°$	—	Entropy change, kJ $mol^{-1}K^{-1}$

References

[1] P. Xu, G.M. Zeng, D.L. Huang, C.L. Feng, S. Hu, M.H. Zhao, C. Lai, Z. Wei, C. Huang, G.X. Xie, Z.F. Liu, Use of iron oxide nanomaterials in wastewater treatment: a review, Sci. Total Environ., 424 (2012) 1–10.
[2] P. Schröder, J. Navarro-Aviñó, H. Azaizeh, A.G. Goldhirsh, S. Digregorio, T. Komives, G. Langergraber, A. Lenz, E. Maestri, A.R. Memon, A. Ranalli, L. Sebastiani, S. Smrcek, T. Vanek, S. Vuilleumier, F. Wissing, Using phytoremediation technologies to upgrade waste water treatment in Europe, Paris Environ. Sci. Pollut. Res., 14 (2007) 490–497.
[3] A. Demirbas, Agricultural based activated carbons for the removal of dyes from aqueous solutions: a review, J. Hazard. Mater., 167 (2009) 1–9.
[4] M.T. Yagub, T.K. Sen, S. Afroze, H.M. Ang, Dye and its removal from aqueous solution by adsorption: a review, Adv. Colloid Interface Sci., 209 (2014) 172–184.
[5] A. El Nemr, O. Abdelwahab, A. El-Sikaily, A. Khaled, Removal of direct blue-86 from aqueous solution by new activated carbon developed from orange peel, J. Hazard. Mater., 161 (2009) 102–110.
[6] S. De Gisi, G. Lofrano, M. Grassi, M. Notarnicola, Characteristics and adsorption capacities of low-cost sorbents for wastewater treatment: a review, Sustainable Mater. Technol., 9 (2016) 10–40.
[7] T. Mahmood, R. Ali, A. Naeem, M. Hamayun, M. Aslam, Potential of used *Camellia sinensis* leaves as precursor for activated carbon preparation by chemical activation with H_3PO_4; optimization using response surface methodology, Process Saf. Environ. Prot., 109 (2017) 548–563.
[8] İ. Demiral, C. Aydın Şamdan, H. Demiral, Production and characterization of activated carbons from pumpkin seed shell by chemical activation with $ZnCl_2$, Desal. Water Treat., 57 (2016) 2446–2454.
[9] O. Pezoti, A.L. Cazetta, I.P.A.F. Souza, K.C. Bedin, A.C. Martins, T.L. Silva, V.C. Almeida, Adsorption studies of methylene blue onto $ZnCl_2$-activated carbon produced from buriti shells (*Mauritia flexuosa* L.), J. Ind. Eng. Chem., 20 (2014) 4401–4407.
[10] D. Angin, Production and characterization of activated carbon from sour cherry stones by zinc chloride, Fuel, 115 (2014) 804–811.
[11] D. Angin, A. Ilci, Removal of 2,4-dichlorophenoxy acetic acid from aqueous solutions by using activated carbon derived from olive-waste cake, Desal. Water Treat., 82 (2017) 282–291.
[12] K.M. Doke, M. Yusufi, R.D. Joseph, E.M. Khan, Comparative adsorption of crystal violet and congo red onto $ZnCl_2$ activated carbon, J. Dispersion Sci. Technol., 37 (2016) 1671–1681.
[13] Ç. Kırbıyık, A.E. Pütün, E. Pütün, Equilibrium, kinetic, and thermodynamic studies of the adsorption of Fe(III) metal ions and 2,4-dichlorophenoxyacetic acid onto biomass-based activated carbon by $ZnCl_2$ activation, Surf. Interfaces, 8 (2017) 182–192.
[14] H. Sayğili, F. Güzel, High surface area mesoporous activated carbon from tomato processing solid waste by zinc chloride activation: process optimization, characterization and dyes adsorption, J. Cleaner Prod., 113 (2016) 995–1004.
[15] A.O. Abo El Naga, M. El Saied, S.A. Shaban, F.Y. El Kady, Fast removal of diclofenac sodium from aqueous solution using sugar cane bagasse-derived activated carbon, J. Mol. Liq., 285 (2019) 9–19.
[16] W. Russ, M. Schnappinger, In: V. Oreopoulou, W. Russ, Utilization of By-Products and Treatment of Waste in the Food Industry, Springer US, New York 2007, pp. 1–13.
[17] FAOSTAT, Crop Statistics, 2019. Available at: http://www.fao.org/faostat/en/#data/QC (accessed November 24, 2019).
[18] USDA, Citrus: World Markets and Trade, USDA Foreign Agricultural Service. Available at: https://www.fas.usda.gov/data/citrus-world-markets-and-trade (accessed November 27, 2019).
[19] K. Rezzadori, S. Benedetti, E.R. Amante, Proposals for the residues recovery: orange waste as raw material for new products, Food Bioprod. Process., 90 (2012) 606–614.
[20] G. Demir, D. Angın, Effect of Activation Temperature on Properties of Activated Carbon from Orange Peel by Zinc Chloride, THERMAM 2014 and 3rd Rostocker Symposium on Thermophysical Properties for Technical Thermodynamics, 2014, pp. 101–106.
[21] T.E. Bektas, D. Angin, S. Gunes, Production and characterization of activated carbon prepared from orange pulp and utilization for the removal of phosphate ions, Fresenius Environ. Bull., 27 (2018) 7973–7982.

[22] S. Yorgun, N. Vural, H. Demiral, Preparation of high-surface area activated carbons from Paulownia wood by $ZnCl_2$ activation, Microporous Mesoporous Mater., 122 (2009) 189–194.
[23] C. Patra, R.M.N. Medisetti, K. Pakshirajan, S. Narayanasamy, Assessment of raw, acid-modified and chelated biomass for sequestration of hexavalent chromium from aqueous solution using *Sterculia villosa* Roxb. shells, Environ. Sci. Pollut. Res., 26 (2019) 23625–23637.
[24] D. Angın, Utilization of activated carbon produced from fruit juice industry solid waste for the adsorption of Yellow 18 from aqueous solutions, Bioresour. Technol., 168 (2014) 259–266.
[25] S. Kumar, S. Narayanasamy, R.P. Venkatesh, Removal of Cr(VI) from synthetic solutions using water caltrop shell as a low-cost biosorbent, Sep. Sci. Technol., 54 (2019) 2783–2799.
[26] M.E. Fernandez, G.V. Nunell, P.R. Bonelli, A.L. Cukierman, Activated carbon developed from orange peels: batch and dynamic competitive adsorption of basic dyes, Ind. Crops Prod., 62 (2014) 437–445.
[27] M.B. Desta, Batch sorption experiments: langmuir and freundlich isotherm studies for the adsorption of textile metal ions onto teff straw (*Eragrostis tef*) agricultural waste, J. Thermodyn., 2013 (2013) 1–6.
[28] A. Khaled, A. El Nemr, A. El-Sikaily, O. Abdelwahab, Removal of direct N blue-106 from artificial textile dye effluent using activated carbon from orange peel: adsorption isotherm and kinetic studies, J. Hazard. Mater., 165 (2009) 100–110.
[29] I. Langmuir, The adsorption of gases on plane surfaces of glass, mica and platinum, J. Am. Chem. Soc., 40 (1918) 1361–1403.
[30] H. Freundlich, Über die adsorption in Lösungen, Z. Phys. Chem., 57 (1907) 385–470.
[31] M.M. Dubinin, L.V. Radushkevich, Equation of the characteristics curve of activated charcoal, Chem. Zentralbl., 1 (1947) 875–890.
[32] M.J. Temkin, V. Pyzhev, Recent modifications to Langmuir isotherms, Acta Physicochim. Sin., 12 (1940) 217–222.
[33] A.M. Aljeboree, A.N. Alshirifi, A.F. Alkaim, Kinetics and equilibrium study for the adsorption of textile dyes on coconut shell activated carbon, Arabian J. Chem., 10 (2017) S3381–S3393.
[34] Y.-S. Ho, Citation review of Lagergren kinetic rate equation on adsorption reactions, Scientometrics, 59 (2004) 171–177.
[35] Y.-S. Ho, Second-order kinetic model for the sorption of cadmium onto tree fern: a comparison of linear and non-linear methods, Water Res., 40 (2006) 119–125.
[36] W.J. Weber, J.C. Morris, Kinetics of adsorption on carbon from solution, J. Sanitary Eng. Div., 89 (1963) 31–60.
[37] M.J.D. Low, Kinetics of chemisorption of gases on solids, Chem. Rev., 60 (1960) 267–312.
[38] A. Ajmani, T. Shahnaz, S. Narayanan, S. Narayanasamy, Equilibrium, kinetics and thermodynamics of hexavalent chromium biosorption on pristine and zinc chloride activated Senna siamea seed pods, Chem. Ecol., 35 (2019) 379–396.
[39] M. Kilic, E. Apaydin-Varol, A.E. Pütün, Adsorptive removal of phenol from aqueous solutions on activated carbon prepared from tobacco residues: equilibrium, kinetics and thermodynamics, J. Hazard. Mater., 189 (2011) 397–403.
[40] F. Kaouah, S. Boumaza, T. Berrama, M. Trari, Z. Bendjama, Preparation and characterization of activated carbon from wild olive cores (oleaster) by H_3PO_4 for the removal of Basic Red 46, J. Cleaner Prod., 54 (2013) 296–306.
[41] D. Das, D. P. Samal, M. BC, Preparation of activated carbon from green coconut shell and its characterization, J. Chem. Eng. Process Technol., 6 (2015) 1–7.
[42] Z. Wang, F. Cuib, Y. Pana, L. Houa, B. Zhanga, Y. Lib, L. Zhu., Hierarchically micro-mesoporous β-cyclodextrin polymers used for ultrafast removal of micropollutants from water, Carbohydr. Polym., 213 (2019) 352–360.
[43] J. Saleem, U. Bin Shahid, M. Hijab, H. Mackey, G. McKay, Production and applications of activated carbons as adsorbents from olive stones, Biomass Convers. Biorefin., 9 (2019) 775–802.
[44] S. Karmaker, M.N. Uddin, H. Ichikawa, Y. Fukumori, T.K. Saha, Adsorption of reactive orange 13 onto jackfruit seed flakes in aqueous solution, J. Environ. Chem. Eng., 3 (2015) 583–592.
[45] R. Malik, D.S. Ramteke, S.R. Wate, Adsorption of malachite green on groundnut shell waste based powdered activated carbon, Waste Manag., 27 (2007) 1129–1138.
[46] J. Ndi Nsami, J. Ketcha Mbadcam, The adsorption efficiency of chemically prepared activated carbon from cola nut shells by $ZnCl_2$ on methylene blue, J. Chem., 2013 (2013) 1–7.
[47] V.K.K. Saravanan, C.P.B. Ushadevi, S.V.N. Selvaraju, Biosorption of Acid Yellow 12 from simulated wastewater by non-viable *T. harzianum*: kinetics, isotherm and thermodynamic studies, Int. J. Environ. Sci. Technol., 16 (2019) 6895–6906.
[48] K.L. Chiu, D.H.L. Ng, Synthesis and characterization of cotton-made activated carbon fiber and its adsorption of methylene blue in water treatment, Biomass Bioenergy, 46 (2012) 102–110.
[49] S.N. Milmile, J.V. Pande, S. Karmakar, A. Bansiwal, T. Chakrabarti, R.B. Biniwale, Equilibrium isotherm and kinetic modeling of the adsorption of nitrates by anion exchange Indion NSSR resin, Desalination, 276 (2011) 38–44.
[50] D. Angın, T.E. Köse, U. Selengil, Production and characterization of activated carbon prepared from safflower seed cake biochar and its ability to absorb reactive dyestuff, Appl. Surf. Sci., 280 (2013) 705–710.
[51] K.Y. Foo, B.H. Hameed, Insights into the modeling of adsorption isotherm systems, Chem. Eng. J., 156 (2010) 2–10.
[52] M.D.G. de Luna, E.D. Flores, D.A.D. Genuino, C.M. Futalan, M.W. Wan, Adsorption of Eriochrome Black T (EBT) dye using activated carbon prepared from waste rice hulls-Optimization, isotherm and kinetic studies, J. Taiwan Inst. Chem. Eng., 44 (2013) 646–653.
[53] M. Arami, N.Y. Limaee, N.M. Mahmoodi, Evaluation of the adsorption kinetics and equilibrium for the potential removal of acid dyes using a biosorbent, Chem. Eng. J., 139 (2008) 2–10.
[54] S. Chen, J. Zhang, C. Zhang, Q. Yue, Y. Li, C. Li, Equilibrium and kinetic studies of methyl orange and methyl violet adsorption on activated carbon derived from *Phragmites australis*, Desalination, 252 (2010) 149–156.
[55] Z. Ayazi, Z.M. Khoshhesab, F.F. Azhar, Z. Mohajeri, Modeling and optimization of adsorption removal of reactive Orange 13 on the alginate–montmorillonite–polyaniline nanocomposite via response surface methodology, J. Chin. Chem. Soc., 64 (2017) 627–639.
[56] R. Zandipak, S. Sobhanardakani, Evaluation of kinetic and equilibrium parameters of $NiFe_2O_4$ nanoparticles on adsorption of reactive Orange Dye from water, Iran. J. Toxicol., 10 (2016) 51–58.
[57] C. Patra, T. Shahnaz, S. Subbiah, S. Narayanasamy, Comparative assessment of raw and acid-activated preparations of novel *Pongamia pinnata* shells for adsorption of hexavalent chromium from simulated wastewater, Environ. Sci. Pollut. Res., 27 (2020) 14836–14851.
[58] T. Calvete, E.C. Lima, N.F. Cardoso, J.C.P. Vaghetti, S.L.P. Dias, F.A. Pavan, Application of carbon adsorbents prepared from Brazilian-pine fruit shell for the removal of reactive orange 16 from aqueous solution: kinetic, equilibrium, and thermodynamic studies, J. Environ. Manage., 91 (2010) 1695–1706.
[59] T. Maneerung, J. Liew, Y. Dai, S. Kawi, C. Chong, C.-H. Wang, Activated carbon derived from carbon residue from biomass gasification and its application for dye adsorption: kinetics, isotherms and thermodynamic studies, Bioresour. Technol., 200 (2016) 350–359.
[60] S. Pap, T. Šolević Knudsen, J. Radonić, S. Maletić, S.M. Igić, M. Turk Sekulić, Utilization of fruit processing industry waste as green activated carbon for the treatment of heavy metals and chlorophenols contaminated water, J. Cleaner Prod., 162 (2017) 958–972.

Supplementary information

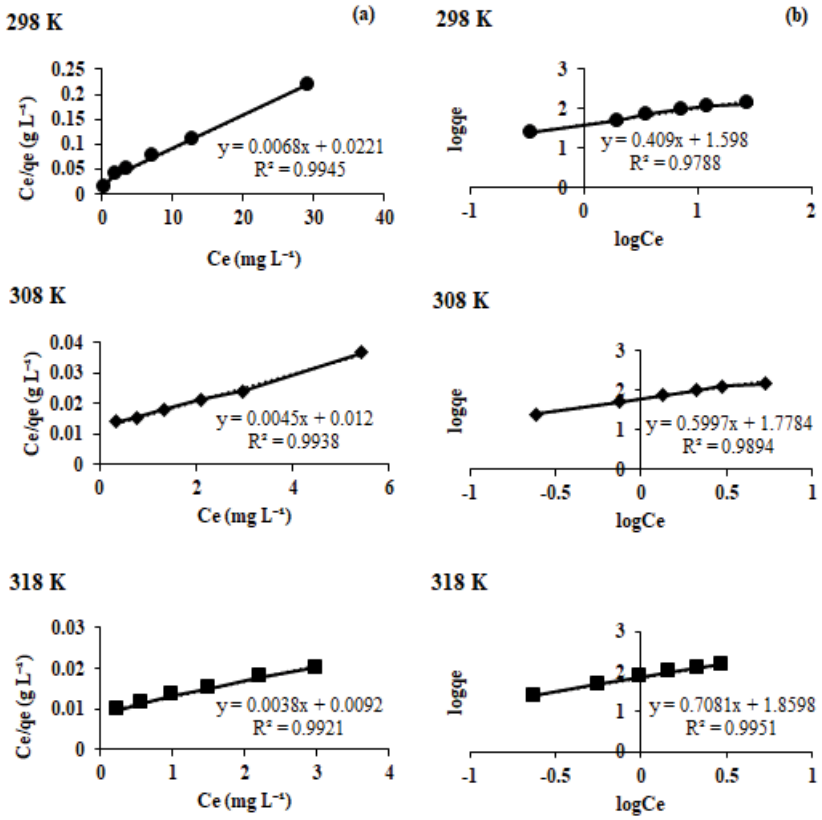

Fig. S1. (a) Langmuir and (b) Freundlich adsorption isotherms of RO-13 onto activated carbons prepared at different temperatures.

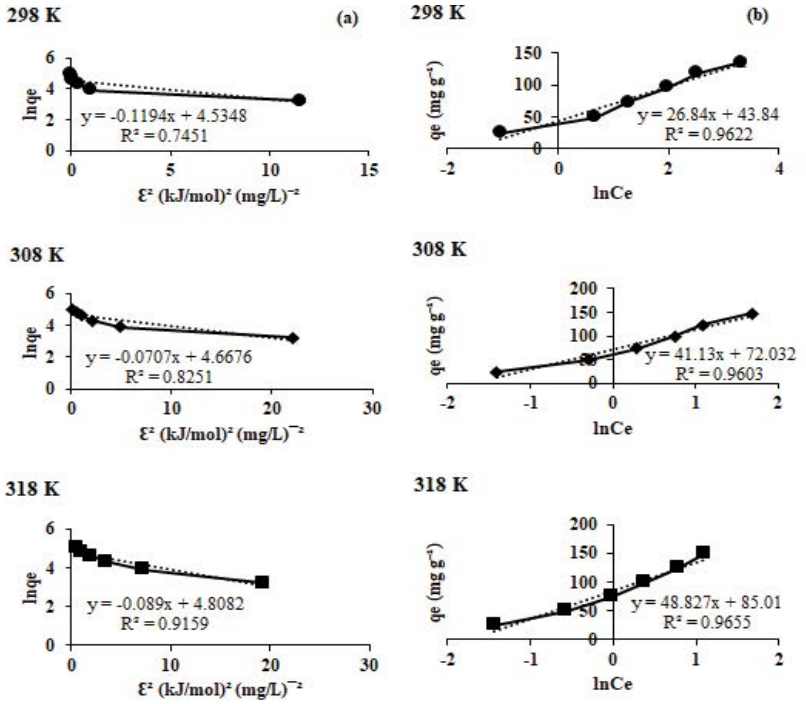

Fig. S2. (a) D–R and (b) Temkin adsorption isotherms of RO-13 onto activated carbons prepared at different temperatures.

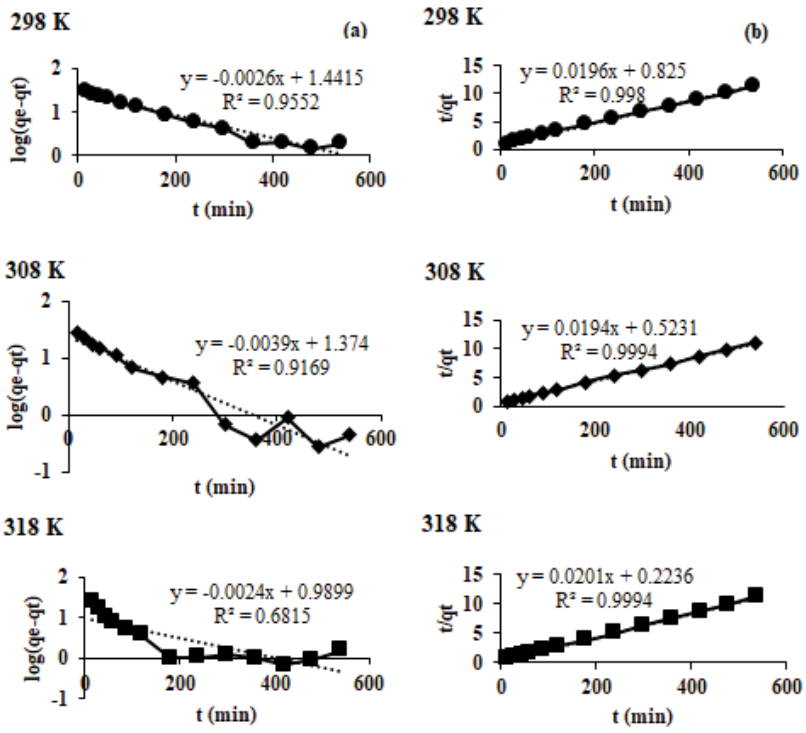

Fig. S3. (a) Pseudo-first-order and (b) pseudo-second-order kinetic models for RO-13 at different temperature.

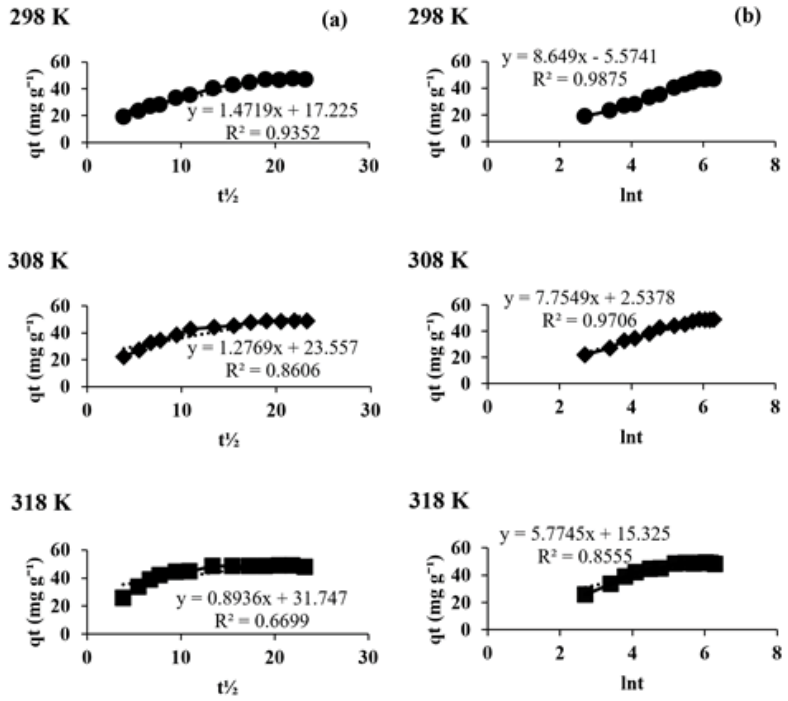

Fig. S4. (a) Intra-particle diffusion and (b) Elovich kinetic models for RO-13 at different temperature.